Current Applied Physics 20 (2020) 828–833

Contents lists available at ScienceDirect

Current Applied Physics

journal homepage: www.elsevier.com/locate/cap

Experimental extraction of stern-layer capacitance in biosensor detection using silicon nanowire field-effect transistors

Sungju Choi[a,1], Hyun-Sun Mo[a,1], Jungmok Kim[a], Seohyeon Kim[a], Seung Min Lee[a], Sung-Jin Choi[a], Dong Myong Kim[a], Dong-Wook Park[b,*], Dae Hwan Kim[a,**]

[a] School of Electrical Engineering, Kookmin University, Seoul, 02707, Republic of Korea
[b] School of Electrical and Computer Engineering, University of Seoul, Seoul, 02504, Republic of Korea

ARTICLE INFO

Keywords:
Stern layer capacitance
Avian influenza detection
Si nanowire
ISFET
TCAD simulation

ABSTRACT

Accurate diagnose of a disease in the early stage is critical to treat the disease properly. To this end, a multitude of biosensors with advanced technologies have been developed to detect the number of biomolecules precisely. In this work, we propose a method for extracting the Stern layer capacitance (C_{stern}) using the experimental data of silicon nanowire ion-sensitive field-effect transistors (ISFETs) to help improve the accurate detection of target molecules. The proposed method was applied to both pH and virus sensing scheme, and the C_{stern} value of pH and a virus were extracted as 32 and 26 μF/cm^2, respectively. These findings indicated that the extracted C_{stern} was affected by the size of the ion and protein, which also was verified by a computer-aided simulation. These insights would be useful in the development of charge-based ISFET biosensors.

1. Introduction

Ion-sensitive field-effect transistors (ISFETs) are a type of biosensor commonly used to detect diseases since being developed by Bergveld in 1970 [1]. With the development of process technologies and detection methods, researchers have investigated various biomedical sensors whose size is comparable to that of their biological target molecules and ions [2,3]. Biomedical sensors using thermometric, magnetic, or fluorescent labeling and parallel optical detection techniques have received much attention because of their high sensitivity [4]. However, these biosensors are complex, expensive, and require time-consuming processes for sample preparation and data processing. To overcome these limitations, nanoscale processes are being carried out to improve device integration, and biosensors using carbon nanotube (CNT) and silicon nanowire (SiNW) field-effect transistors (FET) are being actively studied [5]. SiNW ISFETs are being investigated for their potential application in various sensors, such as pH sensors [3], biosensors [6–9], vapor sensors [10], and gas sensors [11], because of their label-free, real-time detection, and excellent sensitivity. Moreover, SiNWs are readily compatible with existing semiconductor processing technologies as they have easy control of electrical properties, facile surface functionalization with chemical linkers to molecules, and mechanical and chemical robustness for various field of usage [8,12–17].

Recently, FETs have been widely studied as a means of detecting viruses [18]. Many of these studies have focused on increasing the sensitivity of FETs by changing the process conditions and structures such as nanopatterns [2], underlap structures [12], dual gates [14], and floating bodies [19]. Although many of these studies have explained the operating principles in charge-based pH sensors, the sensors for detecting protein molecules have rarely been studies in terms of Stern and diffusion layer. Therefore, several challenges need to be addressed before FETs can be used in commercialized chemical and biomedical sensors.

In this study, we conducted an analysis of the electrostatics of a SiNW FET-based pH and avian influenza (AI) virus functionalized with silica-binding proteins (SBPs). We observed that the electrostatic potential of the Stern layer, diffusion layers, and the functionalized surface groups of the SiNW could be coupled to that of the liquid gate of the SiNW FET-based AI biosensor, which yields the electrical signals of the sensor. In particular, in case of detecting a variety of biomaterials on a single platform, the number of detected biomaterials can be overestimated or underestimated without consideration of the thickness of the stern layer (t_{Stern}), which is considered as a diameter of biomolecule based on Gouy–Chapman–Stern theory [20–22]. We verified our

* Corresponding author.
** Corresponding author.
E-mail addresses: dwpark31@uos.ac.kr (D.-W. Park), drlife@kookmin.ac.kr (D.H. Kim).
[1] S. Choi and H.-S Mo contributed equally to this work.

https://doi.org/10.1016/j.cap.2020.02.021
Received 5 December 2019; Received in revised form 16 February 2020; Accepted 27 February 2020
Available online 05 March 2020
1567-1739/

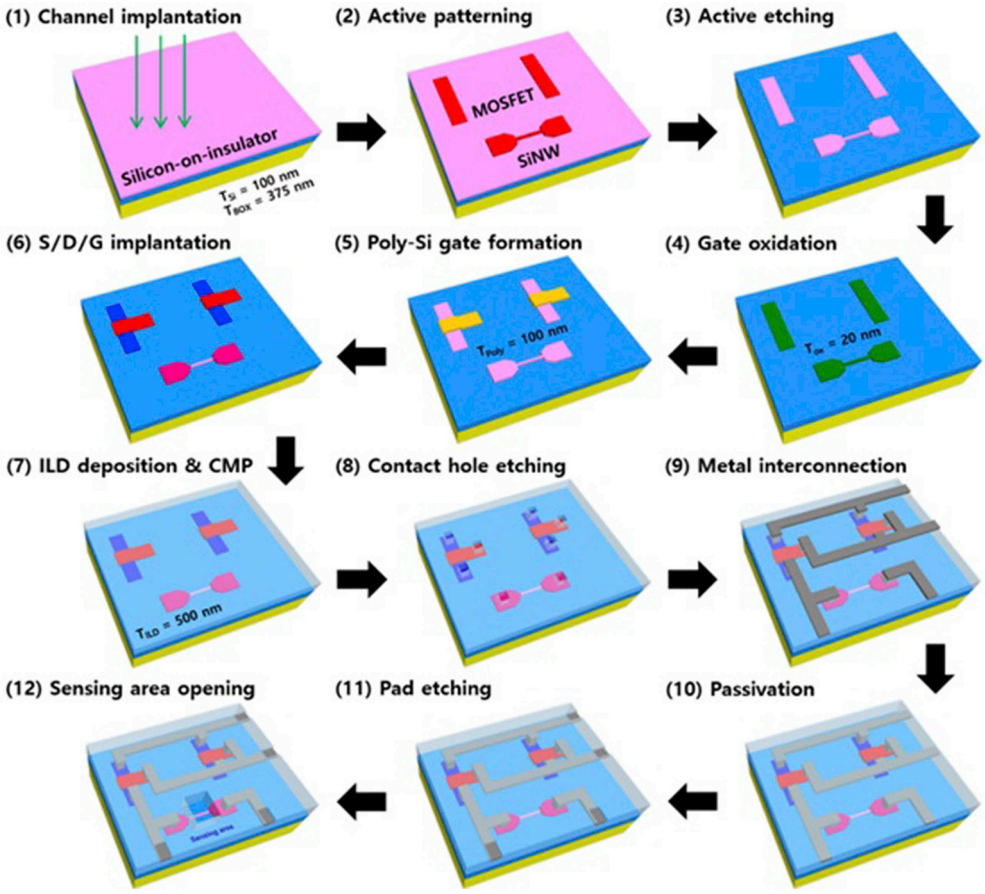

Fig. 1. Fabrication process of SiNW ISFET biosensor.

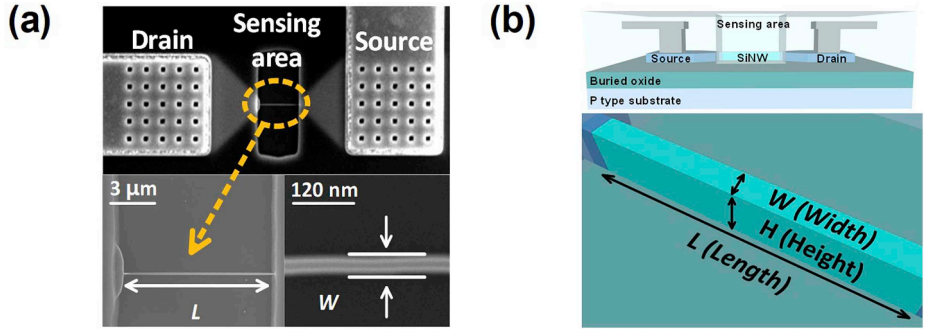

Fig. 2. (a) SEM image of a SiNW FET. (b) Schematic of the demonstrated biosensor composed of an n-type SiNW.

model using a computer-aided design device simulation (TCAD) [23], which gave us insight into how to extract C_{stern} experimentally.

2. Fabrication and experimental procedure

The monolithic integration of the SiNW ISFET was developed as illustrated in Fig. 1. The proposed devices were fabricated on 4×10^{15} cm^{-3} boron-doped (100) silicon on insulator (SOI) wafer (top Si layer = 100 nm and buried oxide = 375 nm). Firstly, the ion implantation was conducted on the Si layer thinned to 80 nm via thermal oxidation for channel doping, p-region (dopant: B^+, energy: 20 keV, dose: 5×10^{13} cm^{-2}) and n-region (P^+ 40 keV 3×10^{13} cm^{-2}). Then, an annealing process was conducted at 950 °C for 30 min for the uniform channel doping of the 80 nm-thick silicon channel. Next, the active region defined mix-and-match process of e-beam and conventional photolithography on the silicon layer. The silicon layer was dry-etched by HBr/O_2 inductively coupled plasma (ICP) for the active formation. The 10 nm thick gate oxide was formed by dry-oxidation at 850 °C. The 100 nm-thick poly-silicon was deposited at 630 °C by low pressure chemical vapor deposition (LPCVD). The poly-silicon on the SiNW was removed by photolithography and ICP dry etching.

Next, by using photo resist (PR) mask which covers only the SiNW channel, the gate (G) and source/drain (S/D) of the SiNW was doped by As^+ ion implantation for n-type S/D/G and $BF_2{}^+$ ion implantation for p-type S/D/G, respectively. A rapid thermal annealing (RTA) was implemented at 900 °C for 10 s to activate the dopants. Inter-layer dielectric oxide (ILD) was deposited by high density plasma CVD (HDPCVD). Photolithography and dry etching formed the contact holes. The aluminum layer was formed on the ILD for metallization. Next, the tetraethyl orthosilicate (TEOS) layer was deposited for passivation, followed by the pads opening by photolithography and dry etching. The oxide layer around the SiNW was removed by using a magnetically

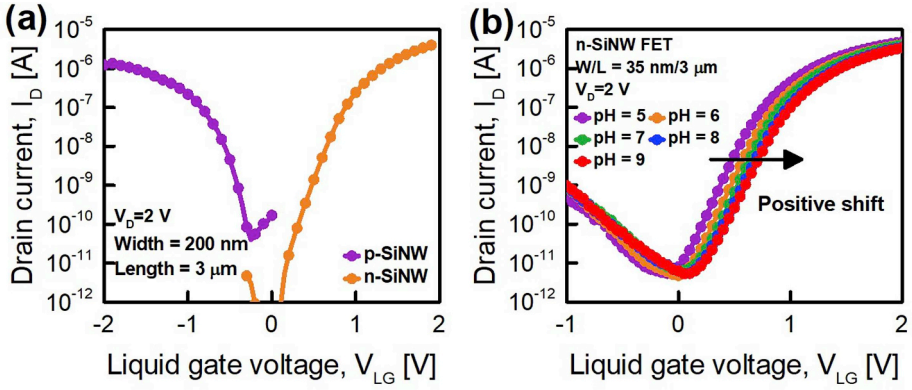

Fig. 3. Measured (a) drain current (I_D)–liquid gate voltage (V_{LG}) curves of the n- and p-type SiNW biosensors (b) transfer characteristic of the n-type SiNW biosensor depending on pH.

enhanced reactive ion etching technique in CHF_3/CF_4 plasma to define the sensing area. Finally, an alloying process was performed to reduce the resistance and improve the performance [24]. Fig. 2(a) shows the top-view SEM image of the fabricated SiNW FET. A schematic of the SiNW biosensor is shown as Fig. 2(b).

3. Results and discussion

The characteristics of the fabricated SiNW biosensor were identified using a semiconductor parameter analyzer under room temperature conditions. To minimize current drift phenomenon, we used fast sweep. Fig. 3(a) displays the drain current (I_D)–liquid gate voltage (V_{LG}) curves under a 2 V drain voltage (V_D) of the n- and p-type SiNW sensors. The extracted threshold voltage (V_T) (n-type = 0.55 V, p-type = −0.65 V) was defined as the value of V_{LG} at an I_D of 10 nA. The sub-threshold swing (*SS*) (n-type = 112 mV/dec and p-type = 103 mV/dec) was extracted from I_D = 0.1 pA to 1 nA. We expect that the relatively large drain off-current in Fig. 3(b) could be improved by optimizing the fabrication process. For the experiments of detecting pH, the SiO_2 surface of the SiNWs was functionalized by 3-aminopropyltriethoxysilane. The I_{DS} of SiNW ISFETs was affected by 0.01 × potassium phosphate buffer solutions (PBS, pH = 7.4) with five different pH values (i.e., pH 5, 6, 7, 8, and 9). Fig. 3(b) described the transfer characteristics of the n-type SiNW FET for the five different pH values. At low pH levels, the $–NH_2$ group was protonated to $–NH_3$, resulting in a positive charge. In contrast, at high pH levels, the −SiOH group was deprotonated to −SiO− and resulted in a negative charge. The average changed V_T (ΔV_T) was slightly smaller at 51 mV per pH (Fig. 4(a)) than the Nernst limit value (59 mV/pH). The surface charge sheet density (Q_{site}) reacted between the surface and the target molecule, and was extracted by using the TCAD simulation applied at each layer (e.g., electrolyte, native oxide, Stern, diffusion, and SiNW layers) [25]. Especially, the thickness of native oxide is 2 nm; the relative permittivity of stern layer is water (6.777), and the effective ionic concentration value is applied to describe the electrolyte (0.01 × PBS) as the intrinsic semiconductor (the intrinsic carrier density (n_i) = 1.03×10^{18} cm^{-3}) [25]. Fig. 4(b) depicts the extracted n_{site} (Q_{site}/q) values. Similarly, the extraction method was applied to an AI virus sensor which utilize the reaction between an antigen and an antibody. We applied a synthetic surface AI antibody (AIa) that was fused with SBPs via recombinant technology to directly fix the antibody onto the silica surface without any further surface modification [14]. Also, we prepared various concentrations of AI and SBP-AIa for the antigen–antibody reaction.

We immersed the fabricated biosensor in various concentrations of SBP-AIa solution that were diluted in PBS at room temperature for 1 h to detect the AI virus molecules through a potential change caused by the antigen–antibody reaction. The sensor was then rinsed with deionized water to remove the non-immobilized sensor, which was then dried under nitrogen gas. The biosensor was prepared to detect various concentrations of the AI antigen (Anti-AI). Antibody binding occurred when the sensor was immersed in a solution containing anti-AI (diluted in 0.01 × PBS), followed by rinsing with deionized water and drying under a nitrogen atmosphere (Fig. 5(a)) [14].

Fig. 5(b) shows the measured transfer curve characteristics of the SiNW biosensor for different Anti-AI concentrations (i.e., 5 ng/mL, 500 ng/mL, and 50 μg/mL) with SBP-AIa (500 μg/mL). The amino acids of proteins in Anti-AI are organic molecules with at least one NH_2 and one COOH (carboxyl) group, which can form long chains *via* the so-called peptide bonds between the NH_2 group from one molecule and the COOH group from another. According to Fig. 5(b), the SiNW effectively felt a larger amount of negative charges and depleted more and more electrons as the Anti-AI concentration increased, resulting in the current decreasing and the FET V_T increasing to a positive V_{LG} direction.

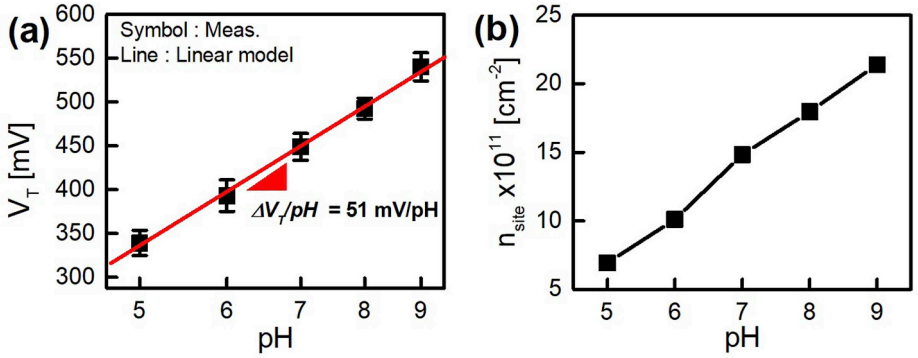

Fig. 4. (a) ΔV_T and (b) n_{site} according to pH (V_T extracted using the constant current method at 10 nA).

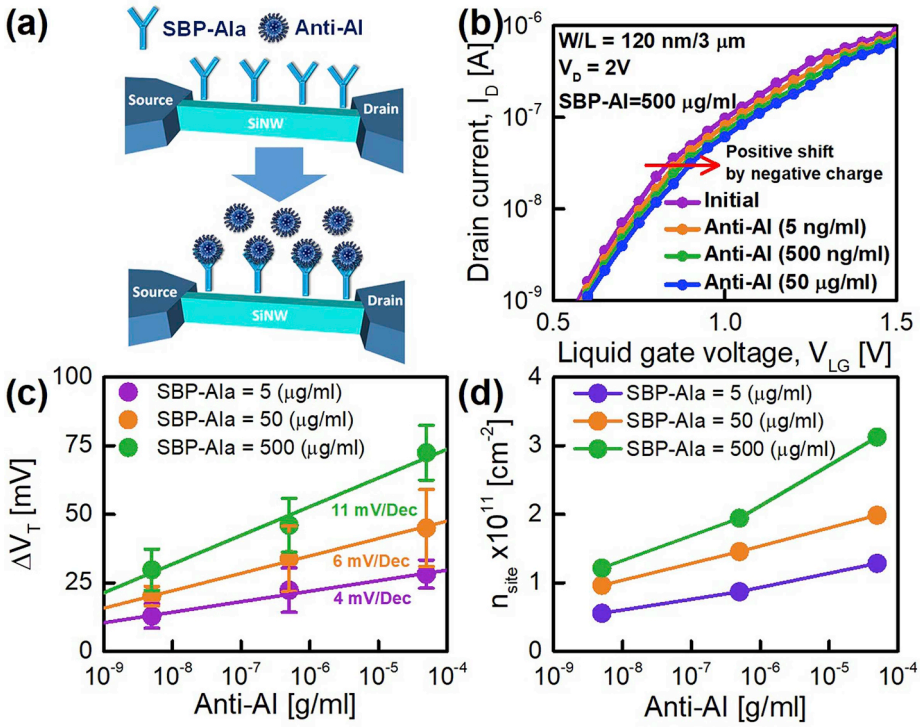

Fig. 5. (a) Antibody–antigen reaction between anti-AI and SBP-AIa. (b) Transfer characteristic of the n-type SiNW biosensor according to the anti-AI molecule concentrations. (c) Changed potential and (d) n_{site} by different concentrations of anti-AI and SBP-AIa of the antigen–antibody reaction.

This mean that the backbone of $–NH_2$ group in Anti-AI was fully in its deprotonated state, and the COOH group was having a net negative charge of the target (Anti-AI) [26].

Various concentrations of AI with different concentrations of SBP-AIa were reacted together (Fig. 5(b)). V_{T0} was defined as V_T after reacting with each concentration of SBP-AIa. Fig. 5(c) depicts the increases in ΔV_T as the concentrations of both SBP-AIa and AI increase. The error bars shown in Fig. 5(c) provide the mean and the standard deviation of six devices. For the SBP-AI concentrations of 5, 50, and 500 μg/mL, the V_T change for the anti-AI concentrations was 4 mV/dec, 6 mV/dec, and 11 mV/dec, respectively. This result indicated that the protein reacted between the AI virus and SBP-AIa and had a negative charge [12,15,19]. Fig. 5(d) shows the n_{site} extracted under various virus concentrations. The relation between Q_{site} and the change in the potential (V_T-V_{T0} = $\Delta\psi_{eo}$) generally follows the Gouy–Chapman–Stern theory shown in Eq. (1) and Fig. 6 [20,22,27–31]:

$$\Delta\psi_{eo} = 2\cdot V_{th}\cdot\sinh^{-1}\left(\frac{Q_{site}}{\sqrt{8\varepsilon_s\varepsilon_0 k_B T n}}\right) + \frac{Q_{site}}{C_{stern}} \quad (1)$$

where, $\Delta\psi_{eo}$ is the change in the total potential; $\Delta\psi_d$ is the change in potential in the diffusion layer; $\Delta\psi_{Cstern}$ is the change in potential in the Stern layer; q is the electronic charge (1.6×10^{-19} C); ε_s is the dielectric constant of the solution (6.7); ε_0 is the permittivity of vacuum; k_B is Boltzmann's constant; T is the absolute temperature (300 K); n is the solution's concentrations [25] ($n = 1.0328 \times 10^{20}$ cm^{-3}); V_{th} is the thermal voltage; C_{ox} is the native oxide capacitance (native oxide thickness = 2 nm); and C_{stern} is the Stern layer capacitance.

Based on the Gouy–Chapman–Stern theory for ISFET-based biosensors, the change in potential caused by Q_{site} can be expressed as the sum of the potential at the diffusion layer, where the counter ion diffusion exists, and that at the Stern layer, where ions cannot exist. Especially, in Stern layer, ions in the electrolyte are inaccessible near the dielectric because they have the finite ionic radius, which cause the steric effects. Therefore, next to surface of dielectric, there are Stern layer where the net ionic charge is essentially empty. The thickness

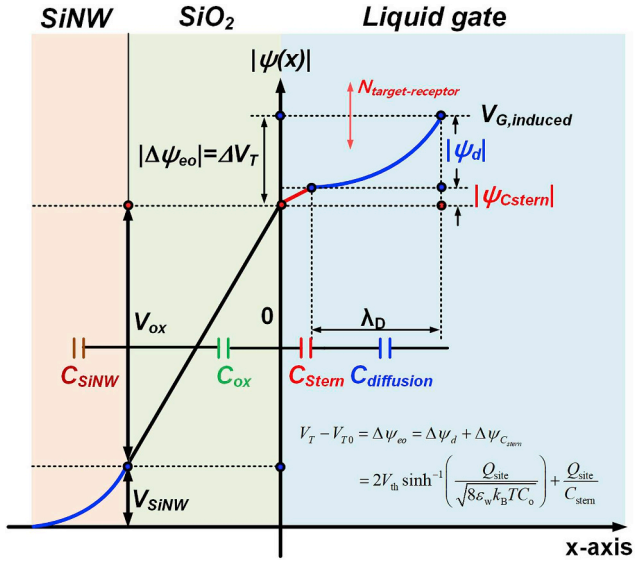

Fig. 6. Schematic of the potential distribution by the reacted Q_{site}.

(t_{Stern}) is generally assumed equal to the cation's atomic radius. A reasonable value of t_{Stern} noticeably reduce the inaccuracies to detect the various biomaterial based on steric effects. For these reasons, it is essential to include a Stern layer in the ISFET model and adjust its value to best fit the experiment.

Using the above-mentioned theory and equation, we performed the TCAD device simulation to show the effect of C_{stern} value. Assuming that C_{stern} is 20, 30, 50, and 100 μF, the simulation results show a considerable difference of ΔV_T as shown Fig. 7(a). When the known parameters of the Gouy–Chapman–Stern theory are input into Eq. (1), Q_{site} can be under estimated or overestimated if incorrect values of C_{stern} are used (Fig. 7(a)) [32].

Fig. 7(b) shows the ΔV_T versus n_{site} plot and the experimentally

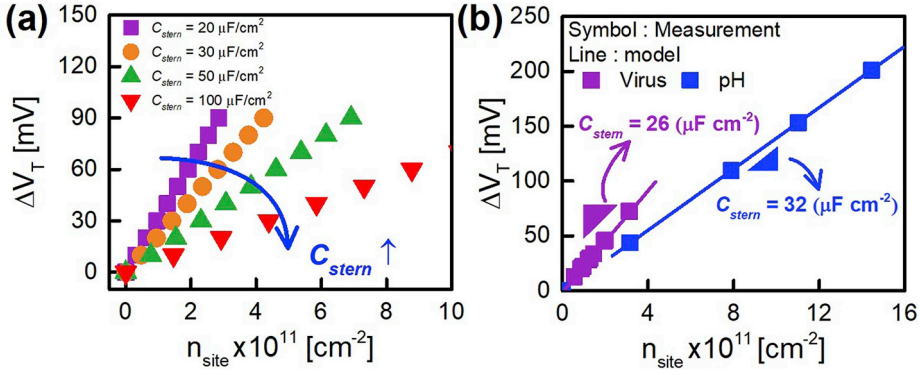

Fig. 7. (a) ΔV_T versus n_{site} plot for various C_{stern} values. (b) Extracted C_{stern} of virus and pH using ΔV_T versus n_{site} plot.

extracted C_{stern} value of the pH and AI virus sensors. From the slope of the plot, the C_{stern} of pH and AI virus were extracted as 32 μF/cm^2 and 26 μF/cm^2, respectively, which is generally in the range of the known value [27,33]. This result can be attributed to t_{stern} being typically determined by the size of target biomaterials (diameter of anti-AI ~120 nm and diameter of H^+ < 0.1 nm) [20,22,27,28]. However, the each C_{stern} by the difference in the size of the ions is not matched. It seems to be the reason that the actual reaction occurs in a specific area rather than evenly across the channel [34]. These results indicate that the accurate extraction of C_{stern} is viable using the proposed analysis and TCAD simulation. The device fabrication and the experimental extraction of n_{site}, and C_{stern} would be of help in developing the ISFET-based biosensor.

4. Conclusion

This study investigated the experimental extraction of C_{stern} of SiNW ISFET as biosensors to detect the target biomolecules. The extracted C_{stern} values from a pH sensor (32 μF/cm^2) and an AI virus sensor (26 μF/cm^2) show that the method can be applied to various biosensors. However, it should be noted that a variety of factors exist that could affect to the detection accuracy such as diffusion capacitance and dielectric capacitance. Also, different surface properties and complex working mechanism in different biosensors necessitate a calibration curve and other schemes to improve the detection accuracy. Nonetheless, we expect the experimental extraction method and the procedure shown in this work could be practically used in various biosensors. The accurate extraction of C_{stern} value will be useful in the development and the characterization of ISFET-based biosensors.

Funding

This work was supported in part of National Research Foundation of Korea (NRF) through the Korean Government, Ministry of Education, Science and Technology (MEST), under Grant 2016R1A5A1012966, Grant 2019M3F3A1A02071845, Grant 18ZB1800, and Grant 2016M3A7B4909668. Also, this work was supported by the 2018 Research Fund of the University of Seoul for Dong-Wook Park.

Acknowledgement

The CAD software was supported by SYNOPSYS and IDEC.

References

[1] P. Bergveld, Development of an ion-sensitive solid-state device for neurophysiological measurements, IEEE Trans. Biomed. Eng. 17 (1970) 70–71, https://doi.org/10.1109/TBME.1970.4502688.
[2] C.K. Jeong, H.M. Jin, J.H. Ahn, T.J. Park, H.G. Yoo, M. Koo, Y.K. Choi, S.O. Kim, K.J. Lee, Electrical biomolecule detection using nanopatterned silicon via block copolymer lithography, Small 10 (2014) 337–343, https://doi.org/10.1002/smll.201301202.
[3] I. Park, Z. Li, A.P. Pisano, R.S. Williams, Top-down fabricated silicon nanowire sensors for real-time chemical detection, Nanotechnology 21 (2010) 015501, , https://doi.org/10.1088/0957-4484/21/1/015501.
[4] R.J. Lipshutz, S.P.A. Fodor, T.R. Gingeras, D.J. Lockhart, High density synthetic oligonucleotide arrays, Nat. Genet. 21 (1999) 20–24, https://doi.org/10.1038/4447.
[5] N. Yang, X. Chen, T. Ren, P. Zhang, D. Yang, Carbon nanotube based biosensors, Sensor. Actuator. B Chem. 207 (2015) 690–715, https://doi.org/10.1016/j.snb.2014.10.040.
[6] Y. Wang, G. Li, Performance investigation for a silicon nanowire FET biosensor using numerical simulation, IEEE Nanotechnol. Mater. Devices Conf. (2010) 81–86, https://doi.org/10.1109/NMDC.2010.5652491.
[7] J. Lee, S. Hwang, B. Choi, J.H. Lee, D. Moon, M. Seol, C.-H. Kim, I. Chung, B. Park, Y.-K. Choi, D.M. Kim, D.H. Kim, S. Choi, A novel SiNW/CMOS hybrid biosensor for high sensitivity/low noise, 2013 IEEE Int. Electron Devices Meet, IEEE, 2013, pp. 14.5.1–14.5.4, , https://doi.org/10.1109/IEDM.2013.6724631.
[8] G. Jayakumar, A. Asadollahi, P.E. Hellström, K. Garidis, M. Östling, Silicon nanowires integrated with CMOS circuits for biosensing application, Solid State Electron. 98 (2014) 26–31, https://doi.org/10.1016/j.sse.2014.04.005.
[9] J. Lee, J. Jang, B. Choi, J. Yoon, J.-Y. Kim, Y.-K. Choi, D. Myong Kim, D. Hwan Kim, S.-J. Choi, A highly responsive silicon nanowire/amplifier MOSFET hybrid biosensor, Sci. Rep. 5 (2015) 12286, https://doi.org/10.1038/srep12286.
[10] Y. Dan, Y. Lu, N.J. Kybert, Z. Luo, A.T.C. Johnson, Intrinsic response of graphene vapor sensors, Nano Lett. 9 (2009) 1472–1475, https://doi.org/10.1021/nl8033637.
[11] M. Shur, M. Hack, Physics of amorphous silicon based alloy field-effect transistors, J. Appl. Phys. 55 (1984) 3831–3842, https://doi.org/10.1063/1.332893.
[12] J.-Y. Kim, J.-H. Ahn, S.-J. Choi, M. Im, S. Kim, J.P. Duarte, C.-H. Kim, T.J. Park, S.Y. Lee, Y.-K. Choi, An underlap channel-embedded field-effect transistor for biosensor application in watery and dry environment, IEEE Trans. Nanotechnol. 11 (2012) 390–394, https://doi.org/10.1109/TNANO.2011.2175006.
[13] J.-Y. Kim, K. Choi, D.-I. Moon, J.-H. Ahn, T.J. Park, S.Y. Lee, Y.-K. Choi, Surface engineering for enhancement of sensitivity in an underlap-FET biosensor by control of wettability, Biosens. Bioelectron. 41 (2013) 867–870, https://doi.org/10.1016/j.bios.2012.08.036.
[14] J.-Y. Kim, J.-H. Ahn, D.-I. Moon, S. Kim, T.J. Park, S.Y. Lee, Y.-K. Choi, A dual-gate field-effect transistor for label-free electrical detection of avian influenza, Bionanoscience 2 (2012) 35–41, https://doi.org/10.1007/s12668-011-0035-0.
[15] J.-H. Ahn, M. Im, T.J. Park, S.Y. Lee, Y. Choi, Label-free and real-time detection of avian influenza using nanowire field effect transistors, J. Biomed. Nanotechnol. 9 (2013) 3–6, https://doi.org/10.1166/jbn.2013.1501.
[16] K. Matsuura, Y. Asano, A. Yamada, K. Naruse, Detection of micrococcus luteus biofilm formation in microfluidic environments by pH measurement using an ion-sensitive field-effect transistor, Sensors 13 (2013) 2484–2493, https://doi.org/10.3390/s130202484.
[17] B. Jin, G.-Y. Lee, C. Park, D. Kim, W. Choi, J.-W. Yoo, J.-C. Pyun, J.-S. Lee, Electrical characteristics and pH response of a parylene-H sensing membrane in a Si-nanonet ion-sensitive field-effect transistor, Sensors 18 (2018) 3892, https://doi.org/10.3390/s18113892.
[18] G.J. Zhang, Y. Ning, Silicon nanowire biosensor and its applications in disease diagnostics: a review, Anal. Chim. Acta 749 (2012) 1–15, https://doi.org/10.1016/j.aca.2012.08.035.
[19] D.-I. Moon, M. Peycelon, J.-Y. Kim, J.-H. Ahn, T. Jung Park, Y.-K. Choi, A biristor based on a floating-body silicon nanowire for biosensor applications, Appl. Phys. Lett. 102 (2013) 043701, , https://doi.org/10.1063/1.4789904.
[20] R.E.G. van Hal, J.C.T. Eijkel, P. Bergveld, A novel description of ISFET sensitivity with the buffer capacity and double-layer capacitance as key parameters, Sensor. Actuator. B Chem. 24 (1995) 201–205, https://doi.org/10.1016/0925-4005(95)85043-0.
[21] L. Bousse, N.F. De Rooij, P. Bergveld, Operation of chemically sensitive field-effect sensors as a function of the insulator-electrolyte interface, IEEE Trans. Electron. Dev. 30 (1983) 1263–1270, https://doi.org/10.1109/T-ED.1983.21284.
[22] S. Layer, V . Electrostatics lecture 26 : compact part of the double layer, Spring (1924) 1–9.

[23] Santa Clara(CA) Silvaco, ATLAS User ' S Manual, (2018).
[24] S. Choi, S. Kim, J. Jang, G. Ahn, J.T. Jang, J. Yoon, T.J. Park, B.-G. Park, D.M. Kim, S.-J. Choi, S.M. Lee, E.Y. Kim, H.S. Mo, D.H. Kim, Implementing an artificial synapse and neuron using a Si nanowire ion-sensitive field-effect transistor and indium-gallium-zinc-oxide memristors, Sensor. Actuator. B Chem. 296 (2019) 126616, https://doi.org/10.1016/j.snb.2019.05.093.
[25] B. Choi, J. Lee, J. Yoon, J. Ahn, T.J. Park, D.M. Kim, D.H. Kim, S. Choi, TCAD-based simulation method for the electrolyte-insulator-semiconductor field-effect transistor, IEEE Trans. Electron. Dev. 62 (2015) 1072–1075, https://doi.org/10.1109/TED.2015.2395875.
[26] L.K. Meixner, S. Koch, Simulation of ISFET operation based on the site-binding model, Sensor. Actuator. B Chem. 6 (1992) 315–318, https://doi.org/10.1016/0925-4005(92)80077-B.
[27] L. Bousse, L. Bousse, N.F. De Rood, P. Bergveld, N.F. De Rooij, P. Bergveld, L. Bousse, N.F. De Rood, P. Bergveld, N.F. De Rooij, P. Bergveld, Operation of chemically sensitive field-effect sensors as a function of the insulator-electrolyte interface, IEEE Trans. Electron. Dev. 30 (1983) 1263–1270, https://doi.org/10.1109/T-ED.1983.21284.
[28] J.P. Valleau, G.M. Torrie, The electrical double layer. III. Modified Gouy – Chapman theory with unequal ion sizes, J. Chem. Phys. 76 (1982) 4623–4630, https://doi.org/10.1063/1.443542.
[29] E. Stern, J.F. Klemic, D.A. Routenberg, P.N. Wyrembak, D.B. Turner-Evans, A.D. Hamilton, D.A. LaVan, T.M. Fahmy, M.A. Reed, Label-free immunodetection with CMOS-compatible semiconducting nanowires, Nature 445 (2007) 519–522, https://doi.org/10.1038/nature05498.
[30] O. Knopfmacher, A. Tarasov, W. Fu, M. Wipf, B. Niesen, M. Calame, C. Schönenberger, Nernst limit in dual-gated Si-nanowire FET sensors, Nano Lett. 10 (2010) 2268–2274, https://doi.org/10.1021/nl100892y.
[31] Y. Cui, Q. Wei, H. Park, C.M. Lieber, Nanowire nanosensors for highly sensitive and selective detection of biological and chemical species, Science 293 (2001) 1289–1292, https://doi.org/10.1126/science.1062711.
[32] A. Bandiziol, P. Palestri, F. Pittino, D. Esseni, L. Selmi, A TCAD-based methodology to model the site-binding charge at ISFET/electrolyte interfaces, IEEE Trans. Electron. Dev. 62 (2015) 3379–3386, https://doi.org/10.1109/TED.2015.2464251.
[33] C. Hughes, L.H. Yeh, S. Qian, Field effect modulation of surface charge property and electroosmotic flow in a nanochannel: stern layer effect, J. Phys. Chem. C 117 (2013) 9322–9331, https://doi.org/10.1021/jp402018u.
[34] M. Uhm, J.-M. Lee, J. Lee, J.H. Lee, S. Choi, B.-G. Park, D.M. Kim, S.-J. Choi, H.-S. Mo, Y.-J. Jeong, D.H. Kim, Ultrasensitive electrical detection of hemagglutinin for point-of-care detection of influenza virus based on a CMP-NANA probe and top-down processed silicon nanowire field-effect transistors, Sensors 19 (2019) 4502, https://doi.org/10.3390/s19204502.